Sustainable Materials and Technologies 42 (2024) e01122

Contents lists available at ScienceDirect

Sustainable Materials and Technologies

journal homepage: www.elsevier.com/locate/susmat

Cationic effect study in acetate-based ionic liquids/ZIF-8 composites for CO_2 sorption

Tiago J. Ferreira [a], Catarina Cabral [a], Thiago O. Carvalho [a], Joana Pais [a], Laura M. Esteves [a], Ludmila P.C. Silva [b], Patrícia M. Reis [a], José M.S.S. Esperança [a,*], Isabel A.A.C. Esteves [a,*]

[a] LAQV/REQUIMTE, Department of Chemistry, NOVA School of Science and Technology, FCT NOVA, 2829-516 Caparica, Portugal
[b] Universidade Federal Fluminense, Departamento de Engenharia Química e de Petróleo, Niterói 24210-240, Brazil

ARTICLE INFO

Keywords:
Ionic liquid (IL)
Metal-organic framework (MOF)
Cationic effect
CO_2 post-combustion separation
IL@MOF composites

ABSTRACT

Several strategies can be considered for the mitigation of carbon dioxide (CO_2) emissions to the atmosphere, and among them is its post-combustion capture/separation from flue gas emitted from coal-fired power plants. In this work, six imidazolium, ammonium- and DABCO-based ionic liquids (ILs) containing the acetate anion were used to impregnate the metal-organic framework (MOF) ZIF-8. The cationic effect was studied to determine how the different cationic families and side alkyl chain size influence the gas sorption performance of the produced IL@MOF composites. The combination of different characterization techniques confirmed IL impregnation, and that the composite materials were microporous and crystalline. Single-component CO_2 and nitrogen (N_2) sorption-desorption equilibrium measurements were performed at 303 K for ZIF-8 and the IL@ZIF-8 materials. At the low-pressure regime (0–1 bar), synergy was observed for the imidazolium-based composites, especially for the one with the long-side alkyl chain. The ideal CO_2/N_2 selectivity was calculated for post-combustion composition, and, at 1 bar, [C_{10}MIM][Ac]@ZIF-8 was over four times more selective than ZIF-8, while the selectivity of [C_2MIM][Ac]@ZIF-8 at this pressure almost tripled when compared to the MOF. A chemical reaction between CO_2 and the imidazolium ILs explained the results.

1. Introduction

In 2022, global energy-related carbon dioxide (CO_2) emissions reached an all-time high of 36.8 Gt [1]. Of all the non-condensable greenhouse gases (GHGs), CO_2 is the most predominant one in the atmosphere [2]. A sharp increase in atmospheric CO_2 concentration that started in the 1960s has intensified the greenhouse effect, which has led to global warming [3]. This phenomenon has been mainly caused by human activity [4], due to the burning of fossil fuels [5], and is responsible for climate change and its visible consequences for life on Earth [6]. In the last decade, efforts to limit global warming have been made. Specifically, net-zero CO_2 emissions targets have been formally adopted to achieve the long-term Paris Agreement temperature goal of limiting the increase in the mean global temperature below 2 °C [7].

Different strategies can be considered to reduce GHGs emissions (specifically, CO_2) and eventually achieve carbon neutrality, namely energy efficiency methods [8], energy transition to renewable sources [9,10], or more direct approaches like direct CO_2 capture from the air [11] and Carbon Capture and Storage (CCS) [12]. Regarding the latter, it is still deemed a crucial strategy for the mitigation of CO_2 emissions [13]. Post-combustion technology is considered a viable method for CO_2 capture/separation from flue gas (a mixture mainly composed of nitrogen (N_2) and CO_2) emitted in large quantities by coal-fired power plants [14].

The most mature technology used in post-combustion CO_2 capture/separation is amine scrubbing, which involves the use of an aqueous ethanolamine solution to chemically absorb the gas [15]. While ethanolamines have fast reaction rates with CO_2, their use has several drawbacks such as amine degradation, equipment corrosion, and high energy requirements for amine regeneration [15]. Therefore, gas adsorption has been considered an alternative technology for post-combustion CO_2 capture/separation [16].

The core of an adsorption-based process is the adsorbent material, and metal-organic frameworks (MOFs) have shown great potential to replace more traditional adsorbents like silica, activated carbons, or zeolites [17–19]. MOFs are a class of materials composed of metal

* Corresponding authors.
E-mail addresses: jmesp@fct.unl.pt (J.M.S.S. Esperança), i.esteves@fct.unl.pt (I.A.A.C. Esteves).

https://doi.org/10.1016/j.susmat.2024.e01122
Received 27 February 2024; Received in revised form 10 August 2024; Accepted 18 September 2024
Available online 19 September 2024

cations/small metallic clusters coordinated to organic ligands that contain potential voids [20]. Their remarkable textural properties (high specific surface areas or large pore volume), thermal and chemical stabilities, high degree of tunability, and high CO_2 adsorption capacity make them appealing candidates for gas adsorption applications [21,22].

To further improve the functionality, selectivity, and stability of MOFs in gas adsorption, MOF-based composite materials have been suggested [23]. Namely, the use of ionic liquids (ILs) that act as a MOF "functionalization" has been proposed. ILs are salts in the liquid state with a low melting point, comprised of organic cations and organic/inorganic anions. Nonflammability, negligible vapor pressure, and a high degree of tunability are among some of their physicochemical properties. Some physisorption and chemisorption ILs (e.g., tetracyanoborate- and carboxylate-based, respectively) show high CO_2 solubility [24,25]. In a work by Kinik et al. [26], the incorporation of the physisorption IL [C_4MIM][PF_6] into the structure of MOF ZIF-8 led to a higher CO_2 sorption capacity up to 0.4 bar, when compared to the pristine ZIF-8. Note that herein the term sorption includes both adsorption and absorption phenomena. Also, the incorporation of the IL more than doubled the ideal CO_2/CH_4 and CO_2/N_2 selectivities (50:50 mixtures) of the composite between 0 and 1 bar, when compared to pristine ZIF-8. A work by our group [27] found that a ~ 7 wt% loading of the chemisorption IL [C_2MIM][Ac] was enough to promote synergistic effects in regard to CO_2 sorption. The [C_2MIM][Ac]@ZIF-8 composite sorbed more CO_2 than the pristine ZIF-8 up until 0.5 bar and an ideal CO_2/CH_4 selectivity (50:50 mixture) increase above 40 % at 0.5 bar of CO_2 partial pressure. In the same work, different physisorption ILs were also impregnated with the same molar IL loading into the structure of ZIF-8. The cationic and anionic effects were studied, but none of these ILs could promote synergistic effects regarding CO_2 sorption capacity. Zeeshan et al. [28] were able to produce a core-shell IL@MOF composite, where the hydrophilic physisorption IL [C_2OHMIM][$N(CN)_2$] was incorporated into the hydrophobic ZIF-8 (~40 wt% IL loading). It is proposed that the difference between the nature of the two materials might play a role in preventing ILs from entering the flexible pore openings of the MOF. The composite material showed higher CO_2 sorption up to 0.4 bar and 45 times higher ideal CO_2/CH_4 selectivity at 1 mbar, when compared to pristine ZIF-8. Finally, Han et al. [29] furthered the core-shell concept in IL@MOF composites by incorporating the hydrophilic IL triethylenetetramine lactate into hydrophobic ZIF-8. Different core-shell configurations were considered (IL inside, outside or on both sides of ZIF-8; the thickness of outer shell was also studied). A high CO_2 sorption capacity was obtained (1.53 mol/kg at 298 K and 1.0 bar), while the uptakes for CH_4 and N_2 were very low. Using the ideal adsorbed solution theory (IAST), selectivities up to 1 bar were predicted to be between 260 and 1990 for CO_2/CH_4 (50:50 mixture) and 1688–5572 for CO_2/N_2 (15:85 mixture).

Acetate-based ILs have been used to produce different IL@MOF composite materials. The chemisorption [C_nMIM][Ac] ILs have a non-linear CO_2 solubility curve and display high CO_2 absorption at low pressures [25,30–32]. These ILs [30,32] have been impregnated into different MOFs. A first work by Mohamedali et al. impregnated [C_2MIM][Ac] and [C_4MIM][Ac] into ZIF-8 [33]. It was found that IL loadings as low at ~8 wt% could promote synergistic effects at different temperatures (303, 313 and 323 K), with all [C_nMIM][Ac]@ZIF-8 composites showing superior or similar CO_2 sorption capacity than then pristine MOF until 1 bar. In this pressure range, the higher the IL loading, the higher the CO_2 sorption capacity was. Afterwards, the decrease of surface area with increasing IL loading negatively impacted the sorption capacity of this gas, when compared to pure ZIF-8. Also, regarding the IL loading effect, there was no obvious trend for ideal CO_2/N_2 selectivities (50:50 mixture) calculated at different temperatures. A second work by Mohamedali et al. impregnated [C_2MIM][Ac] into MOF-177 and MIL-101(Cr) via two different techniques (wet and dry impregnation) [34]. Again, three different IL loadings were considered (10, 20 and 30 wt%). Between 0 and 1 bar, the only [C_2MIM][Ac]@MOF-177 composites that showed relevant synergistic effects were impregnated by the wet impregnation technique, with IL loadings of 10 and 20 wt%. The existence of an optimum IL loading for CO_2 sorption capacity was explained by the fact that excessive IL impregnation in the MOF pores could likely lead to a complete pore blockage and eventually prevent the accessibility of CO_2 to the confined sorption sites. As for the [C_2MIM][Ac]@MIL-101(Cr) composites, the negative impact of the IL impregnation on the CO_2 sorption capacity found for all materials was explained by the decrease in the available pore volume, along with partial coverage of the Cr^{+3} open metal sites by the IL. A final work by Mohamedali et al. impregnated [C_4MIM][Ac] into HKUST-1 [35]. Once again, three different IL loadings were considered (5, 10 and 20 wt%). The CO_2 sorption isotherms obtained at 303, 313 and 323 K revealed that the 5 wt % IL loading was the only one that promoted synergistic effects up to 1 bar. Higher IL loadings had a negative impact on the CO_2 sorption capacity of the composite. These results were explained by the existence of a tradeoff between surface area drop and additional sorption sites created, caused by IL impregnation. In a work by Habib et al., the IL [C_2MIM][Ac] was impregnated into HKUST-1, with a 30 wt% IL loading [36]. The composite showed much lower gas sorption capacity than the pristine MOF. A 6-times improvement in ideal CO_2/N_2 selectivity was found at 1 mbar; at 0.2 bar the composite was less selective than the pristine MOF, explained by a change in the driving forces of surface sorption with increasing pressure. In the work by Nie et al., [C_2MIM][Ac] was impregnated into UiO-66(Zr) [37]. Three different IL loadings were considered (3.5, 5 and 7.5 wt%), with the optimum loading in terms of CO_2 sorption capacity being the lowest one. The composite with 7.5 wt% IL loading already showed lower CO_2 sorption capacity than the pristine MOF. IAST-based CO_2/CH_4 and CO_2/N_2 selectivities were calculated based on the single-component gas sorption isotherms at 298 K, with composites being more selective than the pristine UiO-66(Zr). Finally, in a work by our group, ammonium-based ILs with the acetate anion were incorporated into ZIF-8 [38]. Both [$N_{1\ 2OH\ 2OH\ 2OH}$][Ac]@ZIF-8 and [$N_{2\ 1\ 1\ 4}$][Ac]@ZIF-8 composites showed synergistic effects regarding CO_2 sorption up to 0.3 bar, with the latter material showing an over 50 % increase in ideal CO_2/N_2 selectivity (15:85 mixture) at 1 bar. Both the longer length and apolar nature of the alkyl chains were given as an explanation for the enhanced ideal CO_2/N_2 selectivity of [$N_{2\ 1\ 1\ 4}$][Ac]@ZIF-8.

As presented, besides [C_nMIM]-based ILs, other cationic families are largely unexplored when coupled with the acetate anion, and they may also improve the CO_2 sorption capacity of IL@MOF composites. Therefore in this work, six different ILs were impregnated with the same molar loading into MOF ZIF-8 through a direct contact method. This MOF was chosen because of its chemical stability (even in the presence of water), thermal stability, and microporous nature (pore apertures of 3.4 Å and cavities of 11.6 Å), along with high specific surface area (~1800 m^2/g) and total pore volume (~0.65 cm^3/g) [39]. Always using acetate as the anion, the cationic effect was herein studied to determine how different cationic families with different structures impact sorbent properties such as the gas sorption capacity and selectivity performance of IL@ZIF-8 materials.

Imidazolium-, ammonium- and DABCO-based ILs were synthesized, some reported for the first time to the best of the authors' knowledge, to test the influence of the cation nature. These families were chosen given the possibility of chemical reaction with CO_2 (imidazolium ILs), or structural similarity to amines (ammonium and DABCO ILs). In each cationic family, the influence of the side alkyl chain(s) was also studied, with short chains ($[C_2MIM]^+$, $[N_{2\ 1\ 1\ 4}]^+$, and $[C_2DABCO]^+$) and long chains ($[C_{10}MIM]^+$, $[N_{4\ 1\ 1\ 8}]^+$, and $[C_{12}DABCO]^+$) being considered. The produced IL@MOF composites, apart from the [C_2MIM][Ac]@ZIF-8 one, have never been reported for gas sorption applications.

2. Materials and methods

2.1. Materials

The MOF ZIF-8 (Basolite® Z1200) was purchased from Sigma-Aldrich. The ILs [C_2MIM][Ac] (1-ethyl-3-methylimidazolium acetate, >98 %) and [C_{10}MIM]Cl (1-ethyl-3-methylimidazolium chloride, >98 %) were acquired from IoLiTec GmbH. The other ILs were synthesized and purified in-house, namely [C_{10}MIM][Ac] (1-decyl-3-methylimidazolium acetate, 99 %), [$N_{2\ 1\ 1\ 4}$][Ac] (N-butyl-N-ethyl-N,N-dimethylammonium acetate, 99 %), [$N_{4\ 1\ 1\ 8}$][Ac] (N-butyl-N,N-dimethyl-N-octylammonium acetate, 99 %), [C_2DABCO][Ac] (1-ethyl-1,4-diazabicyclo[2.2.2]octan-1-ium acetate, 99 %) and [C_{12}DABCO][Ac] (1-dodecyl-1,4-diazabicyclo[2.2.2]octan-1-ium acetate, 99 %). The ILs chemical structures are represented in Fig. 1, and their synthesis protocol can be found in the Supporting Information (SI), along with their ^{1}H and ^{13}C NMR spectra (Figs. S1-S8). Regarding the ILs synthesis, N,N-dimethyl-N-butylamine (Sigma-Aldrich, >99 %), 1-bromoethane (Fluka, 98 %), 1-chlorooctane (Sigma-Aldrich, 99 %), 1,4-diazabicyclo [2.2.2]octane (DABCO, Sigma-Aldrich, ≥99 %), 1-bromododecane (Sigma-Aldrich, 97 %) and acetic acid (glacial, Merck, 100 %) were used. Also, for ILs synthesis, anionic resin Amberlite® IRN-78 (Alfa Aesar), ultrapure water produced in-house with a WaterMax W1 equipment (Diwer Technologies), ethanol (Carlo Erba, absolute anhydrous), ethyl acetate (Carlo Erba, 99.9 %) and diethyl ether (Honeywell, ≥99.8 %) were utilized. To obtain the NMR spectra, deuterium oxide (D_2O, Eurisotop, 99.9 % D) was used as the assay solvent. Ethanol (99.9 %, Scharlau) was used for ILs dissolution before their impregnation into the ZIF-8 structure. To obtain the infrared (FT-IR) spectra of solid samples, tablets of potassium bromide (KBr, FT-IR grade, Panreac) were produced. The gases used in sorption-desorption equilibria measurements were CO_2 (99.998 %, Air Liquide), N_2 (>99.998 %, Praxair), and He (≥ 99.999 %, Air Liquide).

2.2. Composites preparation

For this work, [C_2MIM][Ac] was selected as the reference IL, and a 10 wt% loading was adopted. This mass loading is equivalent to a 12.9 mol% loading that was kept constant for all the produced IL@ZIF-8 composites. Given that the same number of IL mole were impregnated, direct and valid comparisons between materials can thus be established.

The production of the IL@ZIF-8 composites followed a previously reported protocol by our group [27]. Before impregnation, all ILs were dried under vacuum (0.1 Pa) for at least 48 h, at 313 K. To produce a given composite, the IL was firstly weighed and dissolved by stirring in ethanol for 15 min at room temperature. Next, 1 g of ZIF-8 (previously degassed for at least 4 h at 373 K to remove adsorbed impurities) was weighed in a different vial. For the impregnation step, the IL solution was added to the MOF vial, capped, and stirred overnight at room temperature. Finally, the vial was uncapped, and ethanol was slowly evaporated at 338 K. When the sample showed a powdery aspect, the composite material was degassed at 373 K for at least 4 h to remove trace amounts of ethanol, and finally stored.

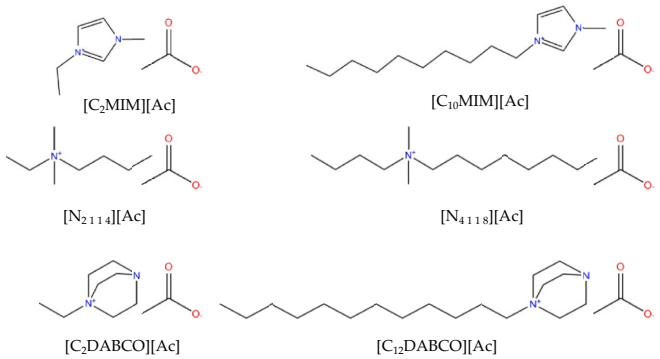

Fig. 1. Chemical structures of the impregnated ILs.

2.3. Samples characterization

2.3.1. Fourier transform infrared (FT-IR) spectroscopy

Infrared spectra of the precursor materials (ZIF-8 and neat ILs) and IL@ZIF-8 composites were obtained with a FT-IR Spectrometer Spectrum Two model (PerkinElmer), between 4000 and 450 cm^{-1} (spectral resolution of 4 cm^{-1}). The Attenuated Total Reflectance (ATR) module was used for the ILs, while the Transmittance module was employed for solid samples. The latter module required the making of KBr tablets containing some milligrams of the sample.

2.3.2. Thermogravimetric analysis (TGA)

The thermograms of the precursor materials and composite materials were obtained with a thermogravimetric analyzer Labsys EVO (Setaram). For a generic assay, the sample was held in an alumina sample pan. Using a 50 mL/min flow of argon (Ar), the sample was first heated up to 373 K (10 K/min heating step). Next, an isothermal step at 373 K for 1 h ensured that all the pre-adsorbed impurities and/or moisture were removed. With this treatment, any subsequent mass loss was exclusively due to material thermal decomposition. A final dynamic step was performed until 1273 K (10 K/min heating rate).

2.3.3. N_2 sorption-desorption equilibrium at 77 K

N_2 sorption-desorption isotherms at 77 K of pristine ZIF-8 and IL@ZIF-8 composites were collected with a static volumetric apparatus ASAP 2010 (Micromeritics). A generic assay started with the degassing of the sample under vacuum at 373 K for at least 8 h, before any sorption-desorption data points were collected. From the isotherms, textural properties of the materials such as total pore and micropore volumes, or BET/Langmuir specific surface areas were determined. Also, with the use of non-local density functional theory (NLDFT) calculations, it was possible to determine the pore size distribution (PSD) of the materials.

2.3.4. Powder X-ray diffraction (PXRD)

Diffractograms of ZIF-8 and composite materials were acquired with an X-ray diffractometer MiniFlex II (Rigaku). The X-ray generator used a Cu radiation source, a voltage of 30 kV and 15 mA of current. For a given material, the assay was run between 2° and 50°, using a step width of 0.02° and 0.5°/min of scanning speed.

2.4. Gas sorption-desorption equilibrium measurements

Single-component CO_2 and N_2 sorption-desorption equilibrium isotherms were obtained at 303 K for pristine ZIF-8 and IL@ZIF-8 composites (0–10 bar). A highly accurate static gravimetric method previously reported elsewhere [27,40,41] was used to experimentally obtain the equilibrium isotherms. The gravimetric apparatus' main feature is a high-accuracy ISOSORP 2000 magnetic-suspension balance (Rubotherm GmbH). Before starting the measurements, samples were degassed for 4 h at 373 K, in situ, and under vacuum. More details concerning the gravimetric apparatus and its schematic can be found elsewhere [27,40,41].

In the literature, the adsorbed gas amount has been reported using net (q_{net}), excess (q_{exc}), or total adsorption (q_t) quantities. Sorption-desorption data of IL@MOF materials can still be reported using these quantities, despite both gas adsorption and absorption occurring. Herein, the net adsorption quantity was used, and it corresponds to the difference between the amount of sorbate found in a measurement cell with and without the presence of the sorbent [42]. The specific net amount sorbed (in mol gas/mass sorbent) is given by

$$q_{net} = \frac{m - m_s - m_h + V_h\rho_g}{m_s\, M_w}, \quad (1)$$

where m is the weighed mass indicated by the balance, m_s is the degassed mass of sorbent inside the sample holder, and m_h and V_h are the mass and volume of the sample holder contributing to buoyancy effects, respectively. Additionally, ρ_g is the gas density at the measurement equilibrium pressure and temperature conditions, and M_w is the molecular weight of the sorbed gas. The advantage of using net quantity is that uncertainty associated with the use of probe molecules (e.g., helium (He), N_2) while determining the required reference state is avoided. However, total sorbed quantity (q_t) is the most used quantity found in the literature. It is possible to relate the three sorbed quantities (in mol gas/mass sorbent) [27].

$$q_t = q_{exc} + V_p\rho_g = q_{net} + (V_p + V_s)\rho_g, \quad (2)$$

where $V_s = 1/\rho_s$ is the specific solid volume of the sorbent that is impenetrable to the sorbate, ρ_s is the skeletal density of the sorbent (determined by He pycnometry, method details found elsewhere [40]), and V_p is the specific total pore volume of the sorbent material (determined from the obtained N_2 sorption-desorption isotherms at 77 K). In the case of the composite materials, one can still use the above formula if both V_p and ρ_s account for the IL presence.

From the collected sorption-desorption data, ideal CO_2/N_2 selectivities were calculated through the accurate description of the equilibrium isotherms by the Sips (Langmuir-Freundlich) and dual-site Sips models. The Sips isotherm model [43] was used to fit the single component sorption-desorption equilibrium data of pristine ZIF-8

$$q_t(P) = \frac{q_s(bP)^{1/n}}{1 + (bP)^{1/n}}, \quad (3)$$

where P is the absolute pressure, q_s is the maximum sorbed amount, b is the affinity parameter, and n is the heterogeneity parameter. For the IL@ZIF-8 composites, as they did not present classical Type I isotherms due to the nature of the impregnated ILs, pure component sorption-desorption equilibrium data were fitted using the dual-site Sips isotherm model [43]

$$q_t(P) = q_{s1}\frac{(b_1P)^{1/n_1}}{1 + (b_1P)^{1/n_1}} + q_{s2}\frac{(b_2P)^{1/n_2}}{1 + (b_2P)^{1/n_2}}, \quad (4)$$

where q_{s1} and q_{s2} are the sorption sites 1 and 2 maximum sorbed amount, respectively, b_1 and b_2 are the affinity constants of the same sorption sites and n_1 and n_2 are the heterogeneity parameters. The ideal selectivities of ZIF-8 and IL@ZIF-8 composites were calculated at 303 K for flue gas composition [44] (15 vol% CO_2 and 85 vol% N_2) following [43].

$$S_{\frac{CO_2}{N_2}} = \frac{q_{t\,CO_2}/q_{t\,N_2}}{p_{CO_2}/p_{N_2}}, \quad (5)$$

where p_{CO_2} and p_{N_2} the partial pressure of each gas.

3. Results and discussion

3.1. FT-IR spectroscopy

The FT-IR spectra of ZIF-8, neat ILs and IL@ZIF-8 composites, shown in Figs. S9-S14 (*See* SI), were compared to confirm IL impregnation. The ZIF-8 spectrum was similar to others reported in the literature [45,46]. If IL-related bands are found in the correspondent IL@ZIF-8 composite spectrum, and not found in the ZIF-8 one, impregnation of the IL into the ZIF-8 structure can be confirmed. At first glance, results showed that the spectra of IL@ZIF-8 composites were very alike to the ZIF-8 one, which means the same chemical bonds were found in the impregnated IL and the MOF. Nevertheless, the spectra of imidazolium-based composites showed two weak IL-related bands between 655 and 615 cm^{-1} (see graphs inset), attributed to rocking in-plane and out-of-plane deformation vibrations of the acetate ion [47]. The ammonium- and DABCO-based IL@ZIF-8 composites also had these bands, but they were very weak and, thus, difficult to observe. Cation-related bands (3200–2800 cm^{-1}) were also observed, particularly if ILs with long alkyl chains were incorporated [47]. FT-IR data confirmed IL impregnation for all composites.

3.2. TGA

The thermal stability of ZIF-8, neat ILs, and the different IL@ZIF-8 composites was assessed through their respective TGA thermograms, shown in Fig. S15 (*See* SI). The precursor materials (ZIF-8 and neat ILs) showed a single stage of mass loss, while all composites showed two stages. The first one corresponded to IL thermal degradation, while the second one was related to the thermal degradation of the 2-methylimidazolate ligand in ZIF-8.

Herein, it was defined a temperature at which mass loss of a degassed sample reached 1 wt%, named starting degradation temperature (T_{start}). It can be seen in Table 1 that pristine ZIF-8 started to degrade at much higher temperatures than the neat ILs and IL@ZIF-8 composites. Imidazolium- and DABCO-based composites showed slightly higher T_{start} values than their respective IL, and the longer the chain the bigger the difference. As for ammonium-based IL@MOF materials, T_{start} values were essentially the same as their respective ILs, irrespective of the alkyl chains size. These two distinct tendencies indicate the presence of IL-MOF interactions, though they differ according to the cationic nature of the IL, which seems to influence the post-impregnation IL arrangement in the ZIF-8 structure.

Calculated TGA thermograms of composite materials were determined from the obtained TGA profiles of ZIF-8 and neat ILs, along with the impregnated IL loading. These thermograms were calculated for a given temperature according to

Table 1
Starting degradation temperatures and remaining sample amount – experimental and expected using Eq. (6) – of ZIF-8, pure ILs, and IL@ZIF-8 composites, at 1273 K.

Sample	IL loading (wt.%)	T_{start} (K)	Experimental remaining sample amount (wt.%)	Expected remaining sample amount (wt.%)
ZIF-8	–	735	50	–
$[C_2MIM][Ac]$	–	462	7	–
$[C_2MIM][Ac]$@ZIF-8	10.0	483	49	46
$[C_{10}MIM][Ac]$	–	456	12	–
$[C_{10}MIM][Ac]$@ZIF-8	15.6	486	43	44
$[N_{2\,1\,1\,4}][Ac]$	–	430	13	–
$[N_{2\,1\,1\,4}][Ac]$@ZIF-8	11.0	427	46	46
$[N_{4\,1\,1\,8}][Ac]$	–	427	9	–
$[N_{4\,1\,1\,8}][Ac]$@ZIF-8	15.1	427	48	44
$[C_2DABCO][Ac]$	–	427	23	–
$[C_2DABCO][Ac]$@ZIF-8	11.6	453	50	47
$[C_{12}DABCO][Ac]$	–	457	17	–
$[C_{12}DABCO][Ac]$@ZIF-8	18.2	504	45	44

$$\text{Calc.wt.\%}|_T = \text{wt.\%}_{\text{ZIF-8}}|_T \times (1 - \text{wt.\%loading}_{\text{IL}}) + \text{wt.\%}_{\text{IL}}|_T \times \text{wt.\%loading}_{\text{IL}} \quad (6)$$

As observed in Fig. S15 (*See* SI), starting from 773 K, the calculated profiles could predict well the experimental ones. In the IL degradation step, a slower degradation rate than the calculated one was observed for all composites (the blue curve is shifted to the right of the green curve). This, together with the fact that composites have similar or higher T_{start} values than their respective neat ILs, indicates that the produced thermal degradation products did not accelerate the decomposition of ZIF-8. This is furthermore supported by the fact that the calculated remaining sample amounts, shown in Table 1, did not significantly differ from the experimental ones.

3.3. Textural properties of IL@ZIF-8 composites

The textural properties of ZIF-8 and IL@ZIF-8 composites were determined from N_2 sorption-desorption equilibrium isotherms obtained at 77 K (Fig. 2 and Fig. S16, *See* SI). A relative pressure of 0.97 was used in the determination of the total pore volume (V_p) of the sorbent materials, and the micropore volume ($V_{micropore}$) was estimated using the Dubinin-Astakhov equation. The BET and Langmuir specific surface areas (A_{BET} and $A_{Langmuir}$, respectively) of the sorbents were also calculated. These properties can be seen in Table 2, alongside the solid matrix density (ρ_s) of each material. The textural properties of ZIF-8 were in accordance with the values reported in the literature [48–50]. The N_2 equilibrium isotherms were all Type I according to the IUPAC classification [51], which indicates the microporous nature of both ZIF-8 and composite materials. This was corroborated by the calculated micropore volumes of these materials, which make up for 85–98 % of the determined total pore volume.

The data in Table 2 indicates the impact of IL impregnation on the textural properties of the composites. When compared to ZIF-8, these materials lost 30–93 % of total pore volume, and BET and Langmuir specific surface areas. This can be explained by IL occupation/blockage of free sorption sites in the ZIF-8 structure. The composite [$N_{4\,1\,1\,8}$][Ac]@ZIF-8, which has an impregnated IL with middle-sized and long alkyl chains, showed the highest textural properties losses. While for all composites ILs blocked/occupied available pore volume (i.e., free sorption sites in the ZIF-8 structure), this was particularly notable for

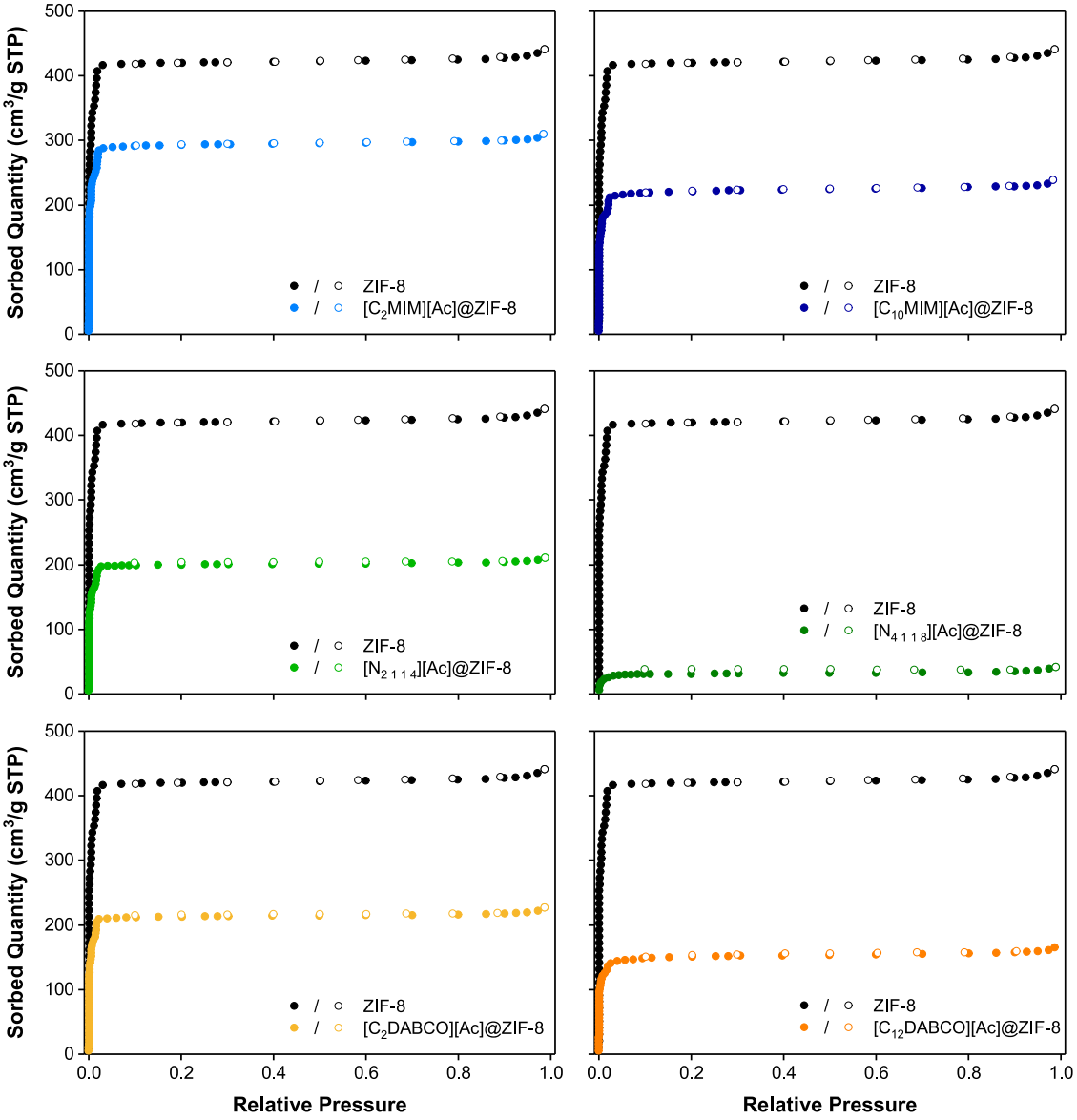

Fig. 2. N_2 sorption-desorption equilibrium isotherms at 77 K of pristine ZIF-8 and all IL@ZIF-composites. Closed and open symbols denote sorption and desorption equilibria data, respectively.

Table 2
Textural properties and skeletal density of ZIF-8 and IL@ZIF-8 composites. The values in brackets are in IL-free basis, expressed per gram of ZIF-8.

Sample	V_p (cm^3/g)	$V_{micropore}$ (cm^3/g)	A_{BET} (m^2/g)	$A_{Langmuir}$ (m^2/g)	ρ_s (g/cm^3)
ZIF-8	0.672	0.655	1862	1926	1.49
[C_2MIM][Ac]@ZIF-8	0.470 (0.522)	0.461 (0.512)	1277 (1419)	1323 (1470)	1.39
[C_{10}MIM][Ac]@ZIF-8	0.360 (0.427)	0.352 (0.417)	936 (1109)	972 (1152)	1.35
[$N_{2\ 1\ 1\ 4}$][Ac]@ZIF-8	0.321 (0.361)	0.313 (0.352)	881 (990)	910 (1022)	1.24
[$N_{4\ 1\ 1\ 8}$][Ac]@ZIF-8	0.060 (0.071)	0.051 (0.060)	129 (152)	138 (163)	1.24
[C_2DABCO][Ac]@ZIF-8	0.343 (0.388)	0.334 (0.378)	935 (1058)	960 (1086)	1.27
[C_{12}DABCO][Ac]@ZIF-8	0.249 (0.304)	0.242 (0.296)	623 (762)	652 (797)	1.25

[$N_{4\ 1\ 1\ 8}$][Ac]@ZIF-8. Interestingly, there were no abrupt textural properties losses for [C_{10}MIM][Ac]@ZIF-8. A possible explanation for this is that, after IL impregnation, the long alkyl chains of [C_{10}MIM]$^+$ cation are packed in such a way that block less pore volume than the same chains in [$N_{4\ 1\ 1\ 8}$]$^+$. This different packing of the chains could be the result of, in likely order of scenarios, higher molar volume of [$N_{4\ 1\ 1\ 8}$]$^+$, nonidentical cation-MOF interactions, and/or different interactions between the long chains and the charged part of the cation.

To truly compare losses between composites, textural properties values should be determined per unit mass of ZIF-8 (in an IL-free basis), as shown in Table 2. All values were still inferior to the ZIF-8 ones, which means that all ILs occupied/blocked available pore volume. From the IL-free textural properties of [$N_{4\ 1\ 1\ 8}$][Ac]@ZIF-8, the IL likely has a different conformation within the ZIF-8 structure when compared to the other ILs.

It should be mentioned that the classical BET data treatment should only be done considering sorption-desorption data points between 0.05 and 0.30 of relative pressure. Usually, this condition cannot be satisfied for microporous materials, so herein the low-pressure range was enlarged for the calculations [51]. Because of this, Langmuir specific surface area is preferred for these materials, with similar albeit slightly overestimated values when compared to the BET ones.

The use of non-local density functional theory (NLDFT) calculations applied to the N_2 sorption-desorption data at 77 K allowed for the determination of the pore size distribution (PSD) of pristine ZIF-8 and composites. As shown in Fig. S17 (*See* SI), most IL@MOF materials had a similar distribution as the MOF precursor, but with less available pore volume. These distributions confirmed the microporous nature of almost all materials, as all pores had $<$20 Å width [51]. It should be noted that, while the PSD of [$N_{4\ 1\ 1\ 8}$][Ac]@ZIF-8 could not be determined from the collected experimental sorption-desorption data points, its N_2 sorption-desorption equilibrium isotherms at 77 K is undeniably Type I, and confirms its microporous nature [51].

3.4. PXRD

To confirm that the ZIF-8 structural integrity was kept after IL impregnation, normalized diffractograms of the MOF and IL@ZIF-8 composites were obtained, as shown in Fig. S18 (*See* SI). The ZIF-8 diffractogram was like others found in previous literature [52,53], and the IL@ZIF-8 ones overlapped it (i.e., peaks positions did not change). Thus, no significant ZIF-8 structural changes occurred due to IL impregnation, with the crystallinity of ZIF-8 being kept.

PXRD diffractograms of IL@ZIF-8 composites showed higher peak intensities when compared to the ZIF-8 one, especially for peaks between 10 and 18°. The increases are more noticeable for composites with long-side alkyl chains (also in short-side alkyl chains, for DABCO-based composites). These differences in peak intensity point to electron density changes after IL impregnation, that result from the formed IL-MOF interactions.

3.5. Sorption performance of IL@ZIF-8 materials

In IL@MOF composites, the gas sorption performance of a material depends on the combination of different factors, namely the chosen MOF/IL system, IL loading, the extent of pore volume loss due to IL occupation/blockage, possible synergistic effects, and the solvent effect. This last one is negligible when ethanol is used as the solvent for IL impregnation in ZIF-8, as shown previously [41], given it does not compromise the sorption capacity of this MOF, as well as its structural integrity. Tables S1-S4 (*See* SI) contain the sorption-desorption equilibrium data of ZIF-8 and IL@ZIF-8 materials produced.

Single-component CO_2 and N_2 sorption-desorption equilibrium isotherms for pristine ZIF-8 and all IL@ZIF-8 composites were measured at 303 K, shown in Fig. 3. These isotherms were all Type I according to IUPAC classification [51] and showed that composites, particularly those with longer alkyl chains, sorbed less gas than ZIF-8 at high pressure. This is due to IL occupation/blockage of available pore volume, which is the predominant factor in this pressure range.

The imidazolium-based composites did not have a linear profile at low pressure. For these materials, the first sorption point indicated a large gas uptake due to the IL presence and the classical Type I shape only started from the second sorption point. This kind of isotherm profile has been previously reported for carboxylate-based IL@MOF materials [33,35] and can be explained by the high CO_2 solubility of these ILs at low pressures (0–1 bar) [25,30]. This proves that ILs, while occupying/blocking pore volume (i.e., free sorption sites), can create new and stronger sorption sites. Interestingly, the [C_{10}MIM]$^+$ cation (with a longer, more apolar chain) was responsible for more CO_2 sorption (apolar gas) than [C_2MIM]$^+$ up until 0.7 bar. This trend, where a long alkyl chain in the 1-alkyl-3-methylimidazolium cation led to slightly higher sorption of this gas, has also been found in [C_nMIM][NTf_2]@ZIF-8 composites [27]. The produced imidazolium-based composites, through synergistic effects, were the only ones where CO_2 sorption at low pressure was superior to pristine ZIF-8.

It should be noted that the mentioned high CO_2 solubility at low pressures in [C_nMIM][Ac] ILs is explained by a chemical reaction between these and CO_2 [30,31,54]. This reaction has been explored in experimental studies [55,56], though the reaction mechanism is disputed. An initial study [57] proposed a reaction mechanism for [C_4MIM][Ac] IL, in which the basicity of the acetate anion was sufficient to deprotonate the imidazolium cation at the C2 position of the ring, producing acetic acid and a highly reactive carbene species. When CO_2 is later absorbed, the carboxylation of the carbene will occur, promoting an abnormal increase in CO_2 sorption [25]. While this reaction likely happens to some extent [58], this simple mechanism has been refuted by subsequent studies [59] and replaced by another that includes the formation of a complex anion [56,60].

More recent mechanisms have been proposed that do not include carbene formation [61]. Irrespective of the mechanism, the reaction between the [C_nMIM][Ac] IL and CO_2 promotes higher CO_2 sorption capacity at low pressures in imidazolium-based ILs [25] and, by extension, in imidazolium-based IL@ZIF-8 composites.

As mentioned before, it is the acidic hydrogen atom found in the imidazolium cation at the C2 position of the ring that will promote the reaction. The fact that no hydrogen atom with such acidity exists in both ammonium- and DABCO-based ILs, despite their cationic structures resembling amines, explains why their respective composites did not

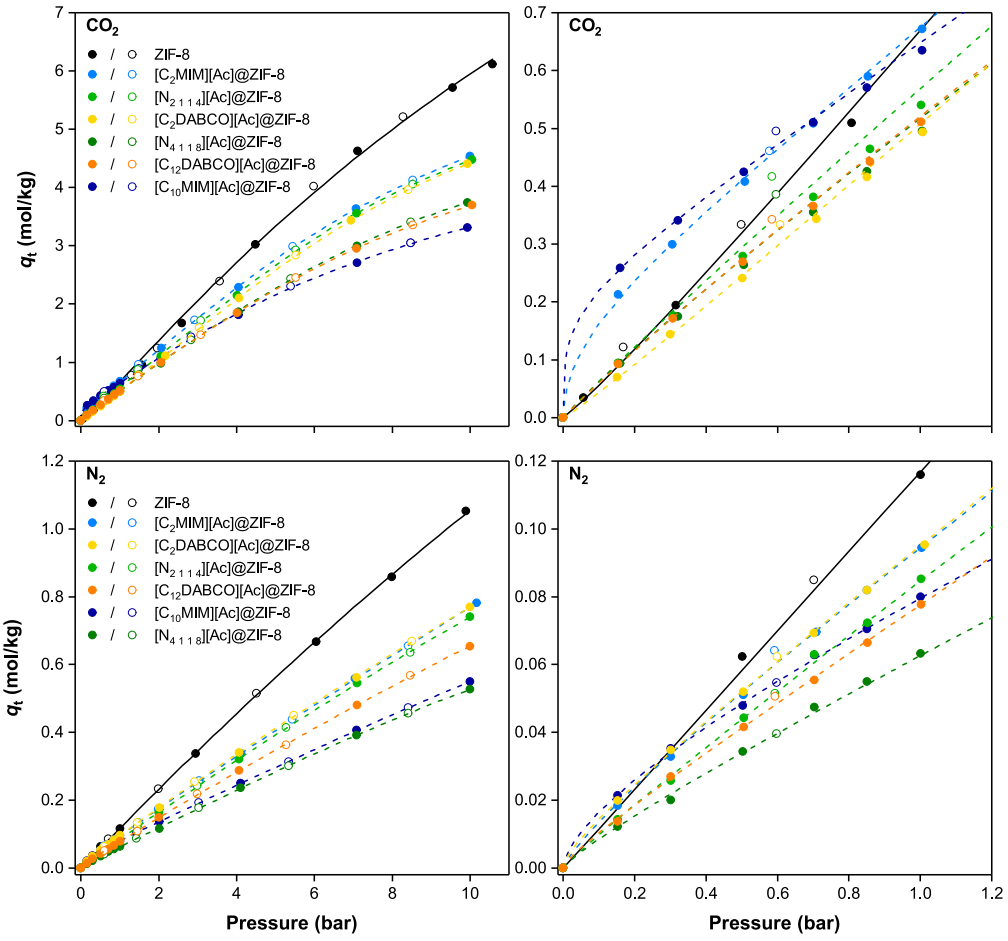

Fig. 3. (Left) Single-component sorption-desorption equilibrium isotherms of CO_2 and N_2 for ZIF-8 and IL@ZIF-8 composites at 303 K. Closed and open symbols denote sorption and desorption data, respectively. Lines represent the Sips (ZIF-8) and dual-site Sips (composites) isotherm models fittings to the experimental data points. (Right) A low-pressure range inset of the data is shown to clarify the goodness of the fittings to the experimental data.

show relevant synergistic effects. Therefore, it is not enough for an impregnated IL to have a basic anion like acetate for synergy between an IL and ZIF-8 to occur at low pressures; a cation that promotes a reversible chemical reaction with CO_2 is also required.

An IL-free basis can be applied to the sorption-desorption data and is revealed in Fig. S19 (*See* SI). The normalization of gas uptake per unit mass of ZIF-8 can once again uncover more information about the IL impact on the sorption capacity of IL@ZIF-8 composites. Using this basis, if ILs did not affect differently the gas sorption capacity, IL-free basis isotherms would collapse into one. Also, because the same amount of IL was impregnated, it is possible to consider at first that ILs could occupy the same pore volume. The N_2 sorption-desorption data 77 K clearly showed that the pore volume is dependent on the impregnated IL. Thus, the gas uptake in IL@MOF materials is dependent on the IL structure, gas solubility, and its arrangement in the MOF structure. Interestingly herein, the ILs with short-side alkyl chains, irrespective of their cation nature, seemed to have the same impact in gas sorption, because their IL-free isotherms were nearly identical at high pressures. For ILs with long-side alkyl chains, the cation nature dictated different impacts on gas sorption capacity. As no IL-free composites isotherms collapsed into the ZIF-8 one, no IL was totally outside the MOF structure and therefore it is furthermore confirmed the occupation/blockage of the available pore volume.

A different way to highlight that ILs structures have an impact on the sorption capacity is to consider the sorption-desorption data per available pore volume. A sorbed amount named q_t/V_p, expressed in mol gas/cm^3 of available pore volume, can be obtained by dividing the gas uptake at a given pressure by the total pore volume of the material. The respective equilibrium isotherms expressed in q_t/V_p can be seen in Fig. S20 (*See* SI). The composite [N_4 1 1 8][Ac]@ZIF-8 showed more gas uptake per available pore volume and proved once again how ILs can tune gas sorption capacity.

The q_t/V_p data of the composites were normalized considering ZIF-8 as the reference, with this normalization being achieved by dividing $q_t/V_p = f(P)$ of a material composite by the respective q_t/V_p of ZIF-8 at the same pressure value. Normalized values are shown in Tables S5 and S6 (*See* SI) for 0.5 and 10 bar, which were deemed as representative values of the low- and high-pressure regimes, respectively. The normalized data are also shown in Fig. 4. Analyzing the quadrants for CO_2 and N_2, all composites showed higher normalized values at low-pressure (green and yellow MAP quadrants). For both pressure regimes, the composite [N_4 1 1 8][Ac]@ZIF-8 showed the highest increases, because this material sorbed gas in the same order of magnitude as the other composites but was revealed to have much lower pore volume. This means that the IL impact in sorption capacity (per available pore volume) is more evident in this material, and not that it sorbed much more than ZIF-8 at both pressure regimes.

To uncover the selectivity performance of the materials, ZIF-8 and IL@ZIF-8 sorption-desorption data were fitted with Sips and dual-site Sips fittings, respectively. The Sips model applies to microporous materials with homogeneous sorbent surfaces [43]. Given that the impregnation of imidazolium-based ILs led to atypical Type I isotherms, the dual-site Sips model was preferred for the composite materials. Moreover, this model considers sorption sites with different energies,

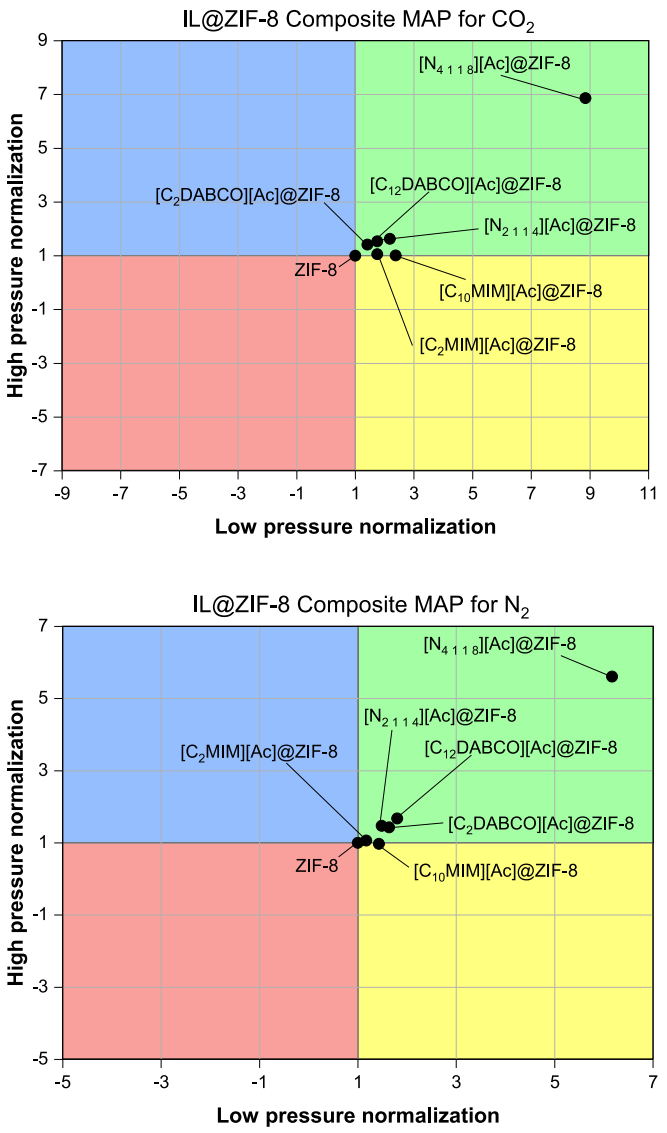

Fig. 4. MAP of IL@ZIF-8 composites for the sorption-desorption equilibrium of CO_2 and N_2 at 303 K. ZIF-8 is the normalization reference assumed in the MAP calculation for both low- and high-pressure normalizations (reference pressures of 0.5 and 10 bar, respectively).

which seems appropriate for these IL@ZIF-8 composites, given the existence of both acetate-based ILs and MOF sorption sites [33,62]. The obtained model fitting parameters can be found in Tables S7 and S8 (*See* SI).

ZIF-8 showed a higher maximum sorbed amount and affinity for CO_2 than for N_2 while presenting a homogeneous system given that n was close to 1. The general trend in composites was that sorption site 1, attributed to ZIF-8 sorption sites, had higher maximum sorbed amounts than those of sorption site 2, attributed to the IL sorption sites. The sole composite in which $q_{s1} > q_{s2}$ was not verified was for N_2 sorption-desorption in [C_2MIM][Ac]@ZIF-8. In many cases, q_{s1} was far superior to q_{s2}, meaning ZIF-8 sorption sites were the ones contributing the most to high-pressure gas sorption. Also, b_1 and b_2 parameters for CO_2 were in general superior to the same parameters for N_2. The sole exception is the b_2 parameter of [C_{10}MIM][Ac]@ZIF-8. This was considered a mathematical artifice caused by trying to find the best fitting for the isotherms of this composite. Since [C_{10}MIM][Ac]@ZIF-8 sorbed more CO_2 than N_2, it is unrealistic that the material shows more affinity towards the latter gas. Finally, in the imidazolium-based composites, the ones that showed atypical Type I CO_2 isotherms, it was found that $n_1 < n_2$, which means the ILs turned the system more heterogeneous. For N_2, $n_1 < n_2$ was verified in the DABCO-based composites, considered also as a mathematical artifice created by the shape of the isotherm.

From the obtained fittings, the ideal CO_2/N_2 selectivity of all the materials considering post-combustion flue gas composition was calculated. The selectivity profiles are shown in Fig. 5 and revealed that all but one composites were more selective than ZIF-8 in the entire pressure range (0–10 bar). In the case of [C_2DABCO][Ac]@ZIF-8, IL impregnation did not improve the selectivity performance of the material, when compared to the original ZIF-8. Imidazolium-based IL@ZIF-8 materials followed a different trend from ZIF-8 and the other composites, with [C_{10}MIM][Ac]@ZIF-8 showing the highest selectivity at 1 bar (pressure value at which flue gas is emitted). This composite showed an over four-time increase in selectivity at this pressure, while [C_2MIM][Ac]@ZIF-8 almost tripled its selectivity. From the ideal CO_2/N_2 selectivity results, impregnated ILs with longer, more apolar side alkyl chains improved the selectivity performance of IL@ZIF-8 composites, when compared to their short chains counterparts. This trend has also been found in [C_nMIM][NTf_2]@ZIF-8 materials [27]. Also at 1 bar, [$N_{4\ 1\ 1\ 8}$][Ac]@ZIF-8 and [C_{12}DABCO][Ac]@ZIF-8 showed 90 % and 51 % increases in selectivity performance, when compared to ZIF-8, although the size of the side alkyl chains had less influence in tuning this sorbent property.

The performance of the produced composites was compared with other IL@ZIF-8 ones found in the literature, as chronologically presented in Table 3. Regarding ideal CO_2/N_2 selectivity, the composite [C_{10}MIM][Ac]@ZIF-8 was found to have a better performance than 77 % of the listed composites, whereas for [C_2MIM][Ac]@ZIF-8 this percentage was 67 %. If one considers the mass IL loadings of composites with high selectivity values, most of them have (or are likely to have) much higher loadings than the imidazolium-based composites produced herein. This means that there is potential in increasing the selectivity (and probably the CO_2 sorption capacity) of the reported [C_nMIM][Ac]@ZIF-8 composites by increasing the amount of impregnated IL.

4. Conclusions

This work studied the cationic effect of six imidazolium-, ammonium- and DABCO-based IL@ZIF-8 composites on gas sorption and ideal CO_2/N_2 selectivity performance.

IL impregnation was confirmed by FT-IR and TGA. The N_2 sorption-

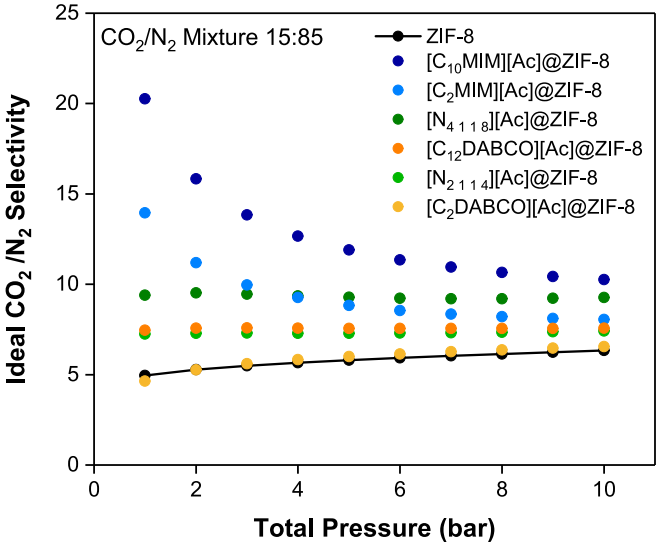

Fig. 5. Ideal CO_2/N_2 selectivity for the pristine ZIF-8 and IL@ZIF-8 composites as a function of the total mixture pressure, determined from the Sips (ZIF-8) and dual-site Sips (composites) adsorption isotherm models of the single-component sorption-desorption isotherms, measured at 303 K and in the pressure range of 0.5–10 bar. The line is a guide-to-the-eye relative to the pristine ZIF-8.

Table 3
Comparison of CO_2 and N_2 sorption capacity and ideal CO_2/N_2 selectivity for ZIF-8 and IL-modified ZIF-8 systems reported in literature. The original nomenclature of each composite was adjusted to the one used herein. Gas sorption capacity values were retrieved at 0.15 bar for CO_2 and 0.85 bar for N_2.

ZIF-8 System	IL loading (wt. %)	Temperature (K)	CO_2 sorption capacity (mol/kg)	N_2 sorption capacity (mol/kg)	Ideal CO_2/N_2 Selectivity	Reference
ZIF-8 [c]	0	303	0.09	0.10	5.0	This work
[C_4MIM][PF_6]@ZIF-8 [a,b,c]	24	298	0.13	0.04	20.4	[26]
	4	298	0.10	0.07	7.7	
[C_4MIM][BF_4]@ZIF-8 [a,b,c]	20	298	0.09	0.06	8.5	[63]
	28	298	0.09	0.04	13.0	
	10	303	0.26	0.09	17.2	
[C_2MIM][Ac]@ZIF-8 [a,c]	20	303	0.54	0.18	17.3	
	26	303	0.68	0.23	16.9	[33]
	8	303	0.19	0.11	9.7	
[C_4MIM][Ac]@ZIF-8 [a,c]	15	303	0.48	0.07	41.6	
	25	303	0.80	0.12	39.5	
[C_4MIM][SCN]@ZIF-8 [a,b,c]	25	298	0.06	0.02	17.9	[64]
[C_4MIM][CH_3SO_3]@ZIF-8 [a,b,c]	25	298	0.09	0.05	10.8	
[C_4MIM][CF_3SO_3]@ZIF-8 [a,b,c]	27	298	0.08	0.08	5.7	[65]
[C_4MIM][CH_3SO_4]@ZIF-8 [a,b,c]	26	298	0.08	0.02	22.0	
[C_4MIM][C_8SO_4]@ZIF-8 [a,b,c]	24	298	0.03	0.03	6.3	
[C_4MIM][$FeCl_4$]@ZIF-8 [c]	13	303	0.05	0.05	5.0	
[C_4MIM]$_2$[$MnCl_4$]@ZIF-8 [c]	18	303	0.04	0.04	7.1	
[C_4MIM]$_2$[$NiCl_4$]@ZIF-8 [c]	18	303	0.05	0.05	5.3	[41]
[C_4MIM]$_2$[$CoCl_4$]@ZIF-8 [c]	18	303	0.04	0.06	4.5	
[C_4MIM]$_2$[$Co(NCS)_4$]@ZIF-8 [c]	20	303	0.03	0.04	4.4	
[TETA][Lac]-ZIF-8-[TETA][Lac] [a,c]	~40	298	1.09	0.01	489.2	
ZIF-8-[TETA][Lac] [a,c]	n.d.	298	0.34	0.07	28.6	
[TETA][Lac]-ZIF-8 [a,c]	n.d.	298	0.44	0.01	368.3	
[TETA][Lac]-ZIF-8-[TETA][Lac]-0 [a,c]	n.d.	298	0.34	0.16	11.9	
[TETA][Lac]-ZIF-8-[TETA][Lac]-0.05 [a,c]	n.d.	298	0.50	0.03	89.7	[29]
[TETA][Lac]-ZIF-8-[TETA][Lac]-0.15 [a,c]	n.d.	298	0.76	0.05	90.7	
[TETA][Lac]-ZIF-8-[TETA][Lac]-0.25 [a,c]	n.d.	298	1.10	0.01	586.5	
[C_2MIM][$N(CN)_2$]@ZIF-8(low) [c]	3	303	0.08	0.08	5.1	
[C_2MIM][$N(CN)_2$]@ZIF-8(high) [c]	6	303	0.08	0.08	5.7	
[C_2MIM][$C(CN)_3$]@ZIF-8(low) [c]	1	303	0.08	0.09	5.2	
[C_2MIM][$C(CN)_3$]@ZIF-8(high) [c]	30	303	0.01	0.002	23.1	[66]
[C_2MIM][NTf_2]@ZIF-8(low) [c]	3	303	0.09	0.09	5.2	
[C_2MIM][NTf_2]@ZIF-8(high) [c]	31	303	0.05	0.04	7.0	
	10	313	0.10	n.a.	2.8	
[C_2MIM][Gly]@ZIF-8(high) [a,d]	20	313	0.24	n.a.	3.6	
	30	313	0.70	n.a.	7.7	
	10	313	0.28	n.a.	2.8	[67]
[C_2MIM][Ala]@ZIF-8(high) [a,d]	20	313	0.32	n.a.	2.3	
	30	313	0.72	n.a.	3.0	
[C_6MIM][$B(CN)_4$]@ZIF-8	11	303	0.06	0.07	5.2	[68]
[$N_{2\ 1\ 1\ 4}$][Ac]@ZIF-8	8	303	0.10	0.07	7.5	
[$N_{1\ 2OH\ 2OH\ 2OH}$][Ac]@ZIF-8	9	303	0.09	0.09	6.1	
[$N_{1\ 2OH\ 2OH\ 2OH}$][NTf_2]@ZIF-8	17	303	0.07	0.07	5.4	[38]
[$N_{2\ 1\ 1\ 2OH}$][AcCys]@ZIF-8	11	303	0.07	0.08	4.8	
[$N_{2\ 1\ 1\ 2OH}$][NTf_2]@ZIF-8	15	303	0.06	0.07	5.3	
[C_2MIM][Ac]@ZIF-8	10	303	0.20	0.08	13.9	
[C_{10}MIM][Ac]@ZIF-8	16	303	0.25	0.07	20.3	
[$N_{2\ 1\ 1\ 4}$][Ac]@ZIF-8	11	303	0.09	0.07	7.2	This work
[$N_{4\ 1\ 1\ 8}$][Ac]@ZIF-8	15	303	0.09	0.05	9.4	
[C_2DABCO][Ac]@ZIF-8	12	303	0.07	0.08	4.6	
[C_{12}DABCO][Ac]@ZIF-8	18	303	0.09	0.07	7.5	

Note that n.d stands for 'not determined' and n.a for 'not available'.
[a] Gas sorption capacity values were retrieved from the graph in the literature.
[b] The sorption capacity of the composite was calculated into mol/kg from cm^3/g.
[c] Selectivity values were determined at 1 bar according to Eq. (5).
[d] Selectivity values were retrieved at 1 bar from the graph in the literature.

desorption equilibrium data at 77 K confirmed the microporous nature of the produced composites and the loss of total pore volume from IL occupation/blockage. The composite [$N_{4\ 1\ 1\ 8}$][Ac]@ZIF-8 had its textural properties significantly affected, while for [C_{10}MIM][Ac]@ZIF-8 and [C_{12}DABCO][Ac]@ZIF-8 this decrease was not as abrupt and explained by different packing of the side alkyl chains. Finally, PXRD data indicated that the ZIF-8 structural integrity and crystallinity were maintained after IL impregnation.

All materials showed Type I isotherms, even though the imidazolium-based composites CO_2 isotherms had an atypical profile at low pressure (0–1 bar). The same composites were the only ones to outperform ZIF-8 in CO_2 sorption at this pressure range, and the synergistic effects were explained by the chemical reaction between the imidazolium ILs and the gas. Despite having structural similarities to amines, ammonium- and DABCO-based ILs were unable to create synergistic effects. Different approaches were used to demonstrate that ILs

impact differently the sorption capacity of the produced IL@ZIF-8 materials, specifically using an IL-free basis and from a pore volume perspective.

The ideal CO_2/N_2 selectivity was calculated for ZIF-8 and IL@ZIF-8 composites considering post-combustion composition. The calculations revealed that, at 1 bar, [C_{10}MIM][Ac]@ZIF-8 was the most selective composite, showing an over four-time increase in selectivity while [C_2MIM][Ac]@ZIF-8 almost tripled its selectivity. The results were explained by stronger interactions between CO_2 (an apolar gas) with longer, more apolar side alkyl chains in 1-alkyl-3-methylimidazolium-based IL@ZIF-8 composites. For the ammonium- and DABCO-based composites, the size of the side alkyl chains had less influence in the tuning of the selectivity performance at low pressure.

In summary, this work studied two rarely- or never-before-explored cationic families, when considering IL@MOF materials for gas sorption. The most natural choice to obtain synergistic effects for CO_2 post-combustion capture/separation pressures is the use of cations with long-side alkyl chains along with acidic hydrogen atoms that, together with a carboxylate-based anion, can promote a reaction with CO_2,

CRediT authorship contribution statement

Tiago J. Ferreira: Writing – review & editing, Writing – original draft, Methodology, Investigation. **Catarina Cabral:** Investigation. **Thiago O. Carvalho:** Writing – review & editing, Investigation. **Joana Pais:** Writing – review & editing, Investigation. **Laura M. Esteves:** Writing – review & editing, Writing – original draft, Methodology, Investigation. **Ludmila P.C. Silva:** Writing – review & editing, Investigation. **Patrícia M. Reis:** Writing – review & editing, Investigation. **José M.S.S. Esperança:** Writing – review & editing, Supervision, Project administration, Methodology, Funding acquisition, Conceptualization. **Isabel A.A.C. Esteves:** Writing – review & editing, Supervision, Project administration, Methodology, Funding acquisition.

Declaration of competing interest

The authors declare that they have no known competing financial interests or personal relationships that could have appeared to influence the work reported in this paper.

Data availability

Data will be made available on request.

Acknowledgments

The authors thank Fundação para a Ciência e Tecnologia, FCT/MCTES (Portugal), for financial support through PhD grants SFRH/BD/139627/2018 and COVID/BD/152969/2023 (T. J. F.), PhD grant 2021.07148.BD (T. O. C.), FCT Investigator contract (2021.00511.CEECIND – P. M. R), and project PTDC/CTM-CTM/30326/2017. The authors also thank the Material Characterization Laboratory (LAMATE/UFF) for obtaining the PXRD diffractograms. Additionally, the work was also partially supported by the Associate Laboratory for Green Chemistry, LAQV, which is funded by national funds from FCT/MCTES (10.54499/LA/P/0008/2020, 10.54499/UIDP/50006/2020, 10.54499/UIDB/50006/2020). The NMR spectrometers are part of The National NMR Facility, supported by FCT/MCTES (Grant RECI/BBB-BQB/0230/2012).

Appendix A. Supplementary data

Supplementary data to this article can be found online at https://doi.org/10.1016/j.susmat.2024.e01122.

References

[1] International Energy Agency, CO2 Emissions in 2022, 2023.
[2] S.A. Montzka, E.J. Dlugokencky, J.H. Butler, Non-CO_2 greenhouse gases and climate change, Nature 476 (2011) 43–50, https://doi.org/10.1038/nature10322.
[3] G. El-Montasser, O. Ben-Salha, A new methodology for assessing the energy use–environmental degradation nexus, Environ. Monit. Assess. 191 (2019) 587, https://doi.org/10.1007/s10661-019-7761-0.
[4] J. Cook, N. Oreskes, P.T. Doran, W.R.L. Anderegg, B. Verheggen, E.W. Maibach, J. S. Carlton, S. Lewandowsky, A.G. Skuce, S.A. Green, D. Nuccitelli, P. Jacobs, M. Richardson, B. Winkler, R. Painting, K. Rice, Consensus on consensus: a synthesis of consensus estimates on human-caused global warming, Environ. Res. Lett. 11 (2016) 048002, https://doi.org/10.1088/1748-9326/11/4/048002.
[5] S.J. Davis, G.P. Peters, K. Caldeira, The supply chain of CO_2 emissions, Proc. Natl. Acad. Sci. USA 108 (2011) 18554–18559, https://doi.org/10.1073/pnas.1107409108.
[6] T.M. Letcher, Why discuss the impacts of climate change?, in: The Impacts of Climate Change Elsevier, 2021, pp. 3–17, https://doi.org/10.1016/b978-0-12-822373-4.00020-3.
[7] M.-T. Huang, P.-M. Zhai, Achieving Paris agreement temperature goals requires carbon neutrality by middle century with far-reaching transitions in the whole society, Adv. Clim. Chang. Res. 12 (2021) 281–286, https://doi.org/10.1016/j.accre.2021.03.004.
[8] S. Akdag, H. Yıldırım, Toward a sustainable mitigation approach of energy efficiency to greenhouse gas emissions in the European countries, Heliyon 6 (2020) e03396, https://doi.org/10.1016/j.heliyon.2020.e03396.
[9] H. Desing, R. Widmer, Reducing climate risks with fast and complete energy transitions: applying the precautionary principle to the Paris agreement, Environ. Res. Lett. 16 (2021) 121002, https://doi.org/10.1088/1748-9326/ac36f9.
[10] M.A. Lima, L.F.R. Mendes, G.A. Mothé, F.G. Linhares, M.P.P. de Castro, M.G. da Silva, M.S. Sthel, Renewable energy in reducing greenhouse gas emissions: reaching the goals of the Paris agreement in Brazil, Environ. Dev. 33 (2020) 100504, https://doi.org/10.1016/j.envdev.2020.100504.
[11] R. Hanna, A. Abdulla, Y. Xu, D.G. Victor, Emergency deployment of direct air capture as a response to the climate crisis, Nat. Commun. 12 (2021) 368, https://doi.org/10.1038/s41467-020-20437-0.
[12] F. Holz, T. Scherwath, P. Crespo del Granado, C. Skar, L. Olmos, Q. Ploussard, A. Ramos, A. Herbst, A 2050 perspective on the role for carbon capture and storage in the European power system and industry sector, Energy Econ. 104 (2021) 105631, https://doi.org/10.1016/j.eneco.2021.105631.
[13] E. Martin-Roberts, V. Scott, S. Flude, G. Johnson, R.S. Haszeldine, S. Gilfillan, Carbon capture and storage at the end of a lost decade, One Earth 4 (2021) 1569–1584, https://doi.org/10.1016/j.oneear.2021.10.002.
[14] Y. Wang, L. Zhao, A. Otto, M. Robinius, D. Stolten, A review of post-combustion CO_2 capture technologies from coal-fired power plants, Energy Procedia 114 (2017) 650–665, https://doi.org/10.1016/j.egypro.2017.03.1209.
[15] X. Wu, Y. Yu, Z. Qin, Z. Zhang, The advances of post-combustion CO_2 capture with chemical solvents: review and guidelines, Energy Procedia 63 (2014) 1339–1346, https://doi.org/10.1016/j.egypro.2014.11.143.
[16] F. Raganati, F. Miccio, P. Ammendola, Adsorption of carbon dioxide for post-combustion capture: a review, Energy Fuel 35 (2021) 12845–12868, https://doi.org/10.1021/acs.energyfuels.1c01618.
[17] C. Jiang, X. Wang, Y. Ouyang, K. Lu, W. Jiang, H. Xu, X. Wei, Z. Wang, F. Dai, D. Sun, Recent advances in metal-organic frameworks for gas adsorption/separation, Nanoscale Adv. 4 (2022) 2077–2089, https://doi.org/10.1039/d2na00061j.
[18] C.A. Trickett, A. Helal, B.A. Al-Maythalony, Z.H. Yamani, K.E. Cordova, O. M. Yaghi, The chemistry of metal–organic frameworks for CO_2 capture, regeneration and conversion, Nat. Rev. Mater. 2 (2017) 17045, https://doi.org/10.1038/natrevmats.2017.45.
[19] Z. Sun, Y. Liao, S. Zhao, X. Zhang, Q. Liu, X. Shi, Research progress in metal-organic frameworks (MOFs) in CO_2 capture from post-combustion coalfired flue gas: characteristics, preparation, modification and applications, J. Mater. Chem. A Mater. 10 (2022) 5174–5211, https://doi.org/10.1039/d1ta07856a.
[20] S.R. Batten, N.R. Champness, X.-M. Chen, J. Garcia-Martinez, S. Kitagawa, L. Öhrström, M. O'Keeffe, M.P. Suh, J. Reedijk, Terminology of metal-organic frameworks and coordination polymers, Pure Appl. Chem. 85 (2013) 1715–1724, https://doi.org/10.1351/PAC-REC-12-11-20.
[21] A.E. Baumann, D.A. Burns, B. Liu, V.S. Thoi, Metal-organic framework functionalization and design strategies for advanced electrochemical energy storage devices, Commun. Chem. 2 (2019) 86, https://doi.org/10.1038/s42004-019-0184-6.
[22] K. Sumida, D.L. Rogow, J.A. Mason, T.M. McDonald, E.D. Bloch, Z.R. Herm, T.-H. Bae, J.R. Long, Carbon dioxide capture in metal—organic frameworks, Chem. Rev. 112 (2012) 724–781, https://doi.org/10.1021/cr2003272.
[23] I. Ahmed, S.H. Jhung, Composites of metal–organic frameworks: preparation and application in adsorption, Mater. Today 17 (2014) 136–146, https://doi.org/10.1016/j.mattod.2014.03.002.
[24] P.J. Carvalho, K.A. Kurnia, J.A.P. Coutinho, Dispelling some myths about the CO_2 solubility in ionic liquids, Phys. Chem. Chem. Phys. 18 (2016) 14757–14771, https://doi.org/10.1039/c6cp01896c.
[25] J. Avila, L.F. Lepre, K. Goloviznina, L. Guazzelli, C.S. Pomelli, C. Chiappe, A. Pádua, M. Costa Gomes, Improved carbon dioxide absorption in double-charged ionic liquids, Phys. Chem. Chem. Phys. 23 (2021) 23130–23140, https://doi.org/10.1039/d1cp02080c.

[26] F.P. Kinik, C. Altintas, V. Balci, B. Koyuturk, A. Uzun, S. Keskin, [BMIM][PF_6] incorporation doubles CO_2 selectivity of ZIF-8: elucidation of interactions and their consequences on performance, ACS Appl. Mater. Interfaces 8 (2016) 30992–31005, https://doi.org/10.1021/acsami.6b11087.

[27] T.J. Ferreira, R.P.P.L. Ribeiro, J.P.B. Mota, L.P.N. Rebelo, J.M.S.S. Esperança, I.A. A.C. Esteves, Ionic liquid-impregnated metal-organic frameworks for CO_2/CH_4 separation, ACS Appl. Nano Mater. 2 (2019) 7933–7950, https://doi.org/10.1021/acsanm.9b01936.

[28] M. Zeeshan, V. Nozari, M.B. Yagci, T. Isık, U. Unal, V. Ortalan, S. Keskin, A. Uzun, Core−Shell type ionic liquid/metal organic framework composite: an exceptionally high CO_2/CH_4 selectivity, J. Am. Chem. Soc. 140 (2018) 10113–10116, https://doi.org/10.1021/jacs.8b05802.

[29] G. Han, N. Yu, D. Liu, G. Yu, X. Chen, C. Zhong, Stepped enhancement of CO_2 adsorption and separation in IL-ZIF-IL composites with shell-interlayer-core structure, AICHE J. 67 (2021) e17112, https://doi.org/10.1002/aic.17112.

[30] A. Yokozeki, M.B. Shiflett, C.P. Junk, L.M. Grieco, T. Foo, Physical and chemical absorptions of carbon dioxide in room-temperature ionic liquids, J. Phys. Chem. B 112 (2008) 16654–16663, https://doi.org/10.1021/jp805784u.

[31] M.B. Shiflett, A. Yokozeki, Phase behavior of carbon dioxide in ionic liquids: [emim][acetate], [emim][Trifluoroacetate], and [emim][acetate] + [emim][Trifluoroacetate] mixtures, J. Chem. Eng. Data 54 (2009) 108–114, https://doi.org/10.1021/je800701j.

[32] W. Shi, R.L. Thompson, E. Albenze, J.A. Steckel, H.B. Nulwala, D.R. Luebke, Contribution of the acetate anion to CO_2 solubility in ionic liquids: theoretical method development and experimental study, J. Phys. Chem. B 118 (2014) 7383–7394, https://doi.org/10.1021/jp502425a.

[33] M. Mohamedali, H. Ibrahim, A. Henni, Incorporation of acetate-based ionic liquids into a zeolitic imidazolate framework (ZIF-8) as efficient sorbents for carbon dioxide capture, Chem. Eng. J. 334 (2018) 817–828, https://doi.org/10.1016/j.cej.2017.10.104.

[34] M. Mohamedali, A. Henni, H. Ibrahim, Investigation of CO_2 capture using acetate-based ionic liquids incorporated into exceptionally porous metal–organic frameworks, Adsorption 25 (2019) 675–692, https://doi.org/10.1007/s10450-019-00073-x.

[35] M. Mohamedali, A. Henni, H. Ibrahim, Markedly improved CO_2 uptake using imidazolium-based ionic liquids confined into HKUST-1 frameworks, Microporous Mesoporous Mater. 284 (2019) 98–110, https://doi.org/10.1016/j.micromeso.2019.04.004.

[36] N. Habib, O. Durak, M. Zeeshan, A. Uzun, S. Keskin, A novel IL/MOF/polymer mixed matrix membrane having superior CO2/N2 selectivity, J. Membr. Sci. 658 (2022) 120712, https://doi.org/10.1016/j.memsci.2022.120712.

[37] S. Nie, F. Chen, T. Shen, T. Wang, N. Di, J. Gao, Incorporation of 1-ethyl-3-methyl-imidazolium acetate into UiO-66 as an efficient sorbent for carbon dioxide capture, New J. Chem. 47 (2023) 2257–2263, https://doi.org/10.1039/d2nj05826j.

[38] T.J. Ferreira, B.A. de Moura, L.M. Esteves, P.M. Reis, J.M.S.S. Esperança, I.A.A. C. Esteves, Biocompatible ammonium-based ionic liquids/ZIF-8 composites for CO_2/CH_4 and CO_2/N_2 separations, Sustain. Mater. Technol. 35 (2023) e00558, https://doi.org/10.1016/j.susmat.2022.e00558.

[39] S.R. Venna, M.A. Carreon, Highly permeable zeolite imidazolate framework-8 membranes for CO_2/CH_4 separation, J. Am. Chem. Soc. 132 (2010) 76–78, https://doi.org/10.1021/ja909263x.

[40] I.A.A.C. Esteves, M.S.S. Lopes, P.M.C. Nunes, J.P.B. Mota, Adsorption of natural gas and biogas components on activated carbon, Sep. Purif. Technol. 62 (2008) 281–296, https://doi.org/10.1016/j.seppur.2008.01.027.

[41] T.J. Ferreira, A.T. Vera, B.A. de Moura, L.M. Esteves, M. Tariq, J.M.S.S. Esperança, I.A.A.C. Esteves, Paramagnetic ionic liquid/metal organic framework composites for CO_2/CH_4 and CO_2/N_2 separations, Front. Chem. 8 (2020) 590191, https://doi.org/10.3389/fchem.2020.590191.

[42] S. Gumma, O. Talu, Net adsorption: a thermodynamic framework for supercritical gas adsorption and storage in porous solids, Langmuir 26 (2010) 17013–17023, https://doi.org/10.1021/la102186q.

[43] D.D. Do, Adsorption Analysis: Equilibria and Kinetics, Imperial College Press, 1998.

[44] L. Liang, C. Liu, F. Jiang, Q. Chen, L. Zhang, H. Xue, H.-L. Jiang, J. Qian, D. Yuan, M. Hong, Carbon dioxide capture and conversion by an acid-base resistant metal-organic framework, Nat. Commun. 8 (2017) 1233, https://doi.org/10.1038/s41467-017-01166-3.

[45] J. Li, Y.N. Wu, Z. Li, B. Zhang, M. Zhu, X. Hu, Y. Zhang, F. Li, Zeolitic imidazolate framework-8 with high efficiency in trace arsenate adsorption and removal from water, J. Phys. Chem. C 118 (2014) 27382–27387, https://doi.org/10.1021/jp508381m.

[46] D. Li, S. Wu, F. Wang, S. Jia, Y. Liu, X. Han, L. Zhang, S. Zhang, Y. Wu, A facile one-pot synthesis of hemin/ZIF-8 composite as mimetic peroxidase, Mater. Lett. 178 (2016) 48–51, https://doi.org/10.1016/j.matlet.2016.04.200.

[47] G. Socrates, The carbonyl group: C=O, in: Infrared and Raman Characteristic Group Frequencies, Third edition, John Wiley & Sons, Chichester, 2004, pp. 115–156.

[48] K.S. Park, Z. Ni, A.P. Côté, J.Y. Choi, R. Huang, F.J. Uribe-Romo, H.K. Chae, M. O'Keeffe, O.M. Yaghi, Exceptional chemical and thermal stability of zeolitic imidazolate frameworks, Proc. Natl. Acad. Sci. USA 103 (2006) 10186–10191, https://doi.org/10.1073/pnas.0602439103.

[49] T. Toyao, M. Fujiwaki, K. Miyahara, T.H. Kim, Y. Horiuchi, M. Matsuoka, Design of zeolitic imidazolate framework derived nitrogen-doped nanoporous carbons containing metal species for carbon dioxide fixation reactions, ChemSusChem 8 (2015) 3905–3912, https://doi.org/10.1002/cssc.201500780.

[50] S. Cao, G. Gody, W. Zhao, S. Perrier, X. Peng, C. Ducati, D. Zhao, A.K. Cheetham, Hierarchical bicontinuous porosity in metal-organic frameworks templated from functional block co-oligomer micelles, Chem. Sci. 4 (2013) 3573–3577, https://doi.org/10.1039/c3sc51336j.

[51] M. Thommes, K. Kaneko, A.V. Neimark, J.P. Olivier, F. Rodriguez-Reinoso, J. Rouquerol, K.S.W. Sing, Physisorption of gases, with special reference to the evaluation of surface area and pore size distribution (IUPAC technical report), Pure Appl. Chem. 87 (2015) 1051–1069, https://doi.org/10.1515/pac-2014-1117.

[52] Y. Song, D. Hu, F. Liu, S. Chen, L. Wang, Fabrication of fluorescent SiO_2@zeolitic imidazolate framework-8 nanosensor for Cu^2+ detection, Analyst 140 (2015) 623–629, https://doi.org/10.1039/c4an01773k.

[53] M. Yurderi, A. Bulut, M. Zahmakiran, M. Gülcan, S. Özkar, Ruthenium(0) nanoparticles stabilized by metal-organic framework (ZIF-8): highly efficient catalyst for the dehydrogenation of dimethylamine-borane and transfer hydrogenation of unsaturated hydrocarbons using dimethylamine-borane as hydrogen source, Appl. Catal. B 160–161 (2014) 534–541, https://doi.org/10.1016/j.apcatb.2014.06.009.

[54] L. Gómez-Coma, A. Garea, A. Irabien, Non-dispersive absorption of CO2 in [emim][EtSO4] and [emim][ac]: temperature influence, Sep. Purif. Technol. 132 (2014) 120–125, https://doi.org/10.1016/j.seppur.2014.05.012.

[55] P.J. Carvalho, V.H. Álvarez, B. Schröder, A.M. Gil, I.M. Marrucho, M. Aznar, L.M.N. B.F. Santos, J.A.P. Coutinho, Specific solvation interactions of CO_2 on acetate and trifluoroacetate imidazolium based ionic liquids at high pressures, J. Phys. Chem. B 113 (2009) 6803–6812, https://doi.org/10.1021/jp901275b.

[56] G. Gurau, H. Rodríguez, S.P. Kelley, P. Janiczek, R.S. Kalb, R.D. Rogers, Demonstration of chemisorption of carbon dioxide in 1,3-Dialkylimidazolium acetate ionic liquids, Angew. Chem. Int. Ed. 50 (2011) 12024–12026, https://doi.org/10.1002/anie.201105198.

[57] E.J. Maginn, Design and Evaluation of Ionic Liquids as Novel CO2 Absorbents, Quaterly Technical Report to U.S, DOE, 2005.

[58] M.B. Shiflett, D.J. Kasprzak, C.P. Junk, A. Yokozeki, Phase behavior of {carbon dioxide + [bmim][Ac]} mixtures, J. Chem. Thermodyn. 40 (2008) 25–31, https://doi.org/10.1016/j.jct.2007.06.003.

[59] S. Stevanovic, A. Podgoršek, A.A.H. Pádua, M.F. Costa Gomes, Effect of water on the carbon dioxide absorption by 1-alkyl-3- methylimidazolium acetate ionic liquids, J. Phys. Chem. B 116 (2012) 14416–14425, https://doi.org/10.1021/jp3100377.

[60] M.B. Shiflett, B.A. Elliott, S.R. Lustig, S. Sabesan, M.S. Kelkar, A. Yokozeki, Phase behavior of CO2 in room-temperature ionic liquid 1-ethyl-3-ethylimidazolium acetate, ChemPhysChem 13 (2012) 1806–1817, https://doi.org/10.1002/cphc.201200023.

[61] J.X. Mao, J.A. Steckel, F. Yan, N. Dhumal, H. Kim, K. Damodaran, Understanding the mechanism of CO2 capture by 1,3 di-substituted imidazolium acetate based ionic liquids, Phys. Chem. Chem. Phys. 18 (2016) 1911–1917, https://doi.org/10.1039/c5cp05713b.

[62] Z. Yang, K.R. Gluesenkamp, A. Frazzica, Equilibrium vapor pressure properties for absorbent and adsorbent materials, Int. J. Refrig. 124 (2021) 134–166, https://doi.org/10.1016/j.ijrefrig.2020.12.013.

[63] B. Koyuturk, C. Altintas, F.P. Kinik, S. Keskin, A. Uzun, Improving gas separation performance of ZIF-8 by [BMIM][BF_4] incorporation: interactions and their consequences on performance, J. Phys. Chem. C 121 (2017) 10370–10381, https://doi.org/10.1021/acs.jpcc.7b00848.

[64] M. Zeeshan, S. Keskin, A. Uzun, Enhancing CO_2/CH_4 and CO_2/N_2 separation performances of ZIF-8 by post-synthesis modification with [BMIM][SCN], Polyhedron 155 (2018) 485–492, https://doi.org/10.1016/j.poly.2018.08.073.

[65] M. Zeeshan, H. Kulak, S. Kavak, H.M. Polat, O. Durak, S. Keskin, A. Uzun, Influence of anion size and electronic structure on the gas separation performance of ionic liquid/ZIF-8 composites, Microporous Mesoporous Mater. 306 (2020) 110446, https://doi.org/10.1016/j.micromeso.2020.110446.

[66] P. Ortiz-Albo, T.J. Ferreira, C.F. Martins, V. Alves, I.A.A.C. Esteves, L. Cunha-Silva, I. Kumakiri, J. Crespo, L.A. Neves, Impact of ionic liquid structure and loading on gas sorption and permeation for ZIF-8-based composites and mixed matrix membranes, Membranes (Basel) 12 (2022) 13, https://doi.org/10.3390/membranes12010013.

[67] F.A. Philip, A. Henni, Enhancement of post-combustion CO_2 capture capacity by incorporation of task-specific ionic liquid into ZIF-8, Microporous Mesoporous Mater. 330 (2022) 111580, https://doi.org/10.1016/j.micromeso.2021.111580.

[68] T.J. Ferreira, L.M. Esteves, J.M.S.S. Esperança, I.A.A.C. Esteves, Unveiling the temperature influence on the Sorptive behaviour of ZIF-8 composite materials impregnated with [CnMIM][$B(CN)_4$] ionic liquids, Processes 10 (2022) 247, https://doi.org/10.3390/pr10020247.